Chapter 4

Zeolite-Templated Carbon: Characterization and Hydrogen Adsorption

4.1 Overview

4.1.1 Background

Carbons with remarkably high surface areas (up to ~3000 m^2 g^{-1}) can be made by conventional chemical activation, among other methods. However, weak hydrogen binding interactions (typically 4-6 kJ (mol H_2)$^{-1}$) limit the effective use of carbon materials to cryogenic temperatures and it is predicted that an ideal heat of adsorption for effective storage near ambient conditions is ~15 kJ mol^{-1}.[1] At 77 K, the Gibbs excess hydrogen uptake in carbon sorbents increases until a maximum value is reached, typically between 1-4 MPa; this value correlates linearly with the specific surface area of the material. "Chahine's rule" predicts ~2 wt% excess uptake of hydrogen, and is valid for a large number of different materials.[2, 3] This capacity is consistent with the theoretical value expected for hydrogen adsorbed in a $\sqrt{3}$ configuration on double-sided graphene sheets. Deviations from this trend are usually explained by increased or decreased surface binding interactions for a given surface chemistry or pore character, or by inaccuracies in measurement techniques.[4]

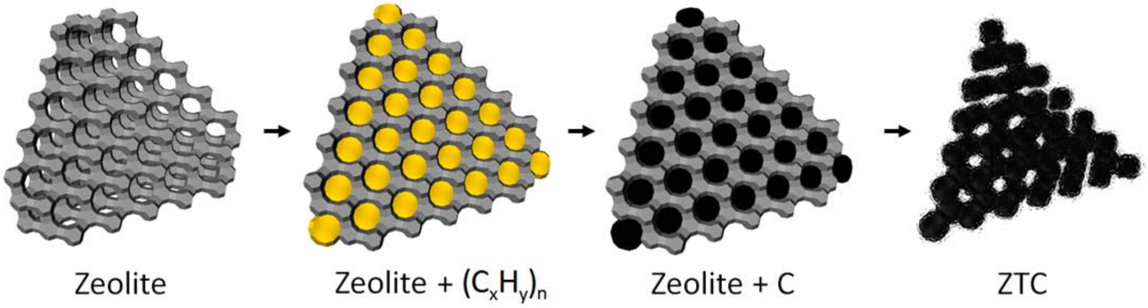

Figure 4.1. A schematic of template-carbonization in a porous zeolite framework, to produce zeolite-templated carbon (ZTC).

4.1.2 High-Pressure Hydrogen Storage

Significant hydrogen sorption capacity at or near room temperature is an important target for candidate storage materials, and numerous strategies to enhance adsorption in carbons have been proposed (e.g., “spillover,” light-atom doping, etc.), but none has yet proven to be a viable technology. Since adsorption of hydrogen at room temperature is very weak, excess uptake in physisorbent materials at modest pressures (<10 MPa) is usually below 1 wt%. There is no general rule relating specific surface area to excess hydrogen uptake capacity at 298 K because a Gibbs surface excess maximum is not achieved. However, hydrogen uptake at a given pressure and 298 K is indeed known to be linearly correlated with specific surface area: ~0.2 wt% excess uptake of hydrogen per 1000 $m^2 g^{-1}$ at 6.5 MPa,[3] for example, an order of magnitude lower than at 77 K.

4.1.3 Zeolite-Templated Carbons

Template carbonization, among other methods of structural control, has also been explored as a technique to produce carbonaceous materials with exceptionally large specific surface area and finely tuned porosity.[5-12] It was reported in 2009 that a particular class of templated materials, zeolite-templated carbons (ZTCs), exhibits remarkable hydrogen storage capacities at room temperature under high-pressure conditions (10-34 MPa).[7] This result was promising for applications of hydrogen storage at room temperature where modestly high pressures are not a barring limitation, and was highly relevant for mobile vehicle applications since hydrogen delivery has already been established up to 70 MPa on the public market (e.g., at the UC Irvine hydrogen station, since 2006).

The reported substantial increase of hydrogen uptake in ZTC "P7(2)-H" could not be explained by surface area alone; the uptake in ZTCs exceeded that of commercially available superactivated carbon of similar surface area, Maxsorb® MSC-30, by nearly 100% at 34 MPa. Extremely narrow microporosity in ZTCs was credited with the improvement, exhibiting optimal pore size for the accommodation of two layers of hydrogen in each pore.[8] However, heats of adsorption in these ZTCs did not show an increase, remaining below 8 kJ mol^{-1}, and the lack of any substantial changes to the thermodynamics is consistent with this explanation. Additionally, BET surface area is notoriously susceptible to error in highly microporous materials such as ZTCs, and may be a significant source of error in the characterization of uptake capacity per surface area at room temperature.

4.1.4 Further Investigation

Measurements of hydrogen adsorption in sorbent materials beyond 15 MPa are few, and most tend towards a plateau beyond 10 MPa at room temperature, while ZTCs are reported to continually increase in this high-pressure regime.[7] Further investigation of this effect was undertaken to ascertain the nature of this anomalous behavior. In the present study, high surface area carbon sorbents were prepared by the zeolite-templating method; materials with BET surface areas of up to 3600 m^2 g^{-1} were produced in multi-gram quantities. Hydrogen uptake measurements of these materials at 77, 87, and 298 K were performed with multiple instruments to assess the viability of ZTCs as hydrogen storage materials for room temperature applications. A specially designed volumetric apparatus was constructed for this work and commissioned for measurements up to 70 MPa.

4.2 Materials Synthesis

To characterize the potentially unique hydrogen adsorption in ZTCs, materials which had properties meeting or exceeding those used in the previous report were necessary. It was found that synthesis of materials up to ~3000 m^2 g^{-1} was readily accomplished with simple laboratory infrastructure, but a limit was reached. High template fidelity was fully realized when experiments were performed together with HRL Laboratories using a converted CVD apparatus which could perform heating under high vacuum or in high purity inert gas conditions: materials with surface areas up to 3600 m^2 g^{-1} were synthesized. The method was readily scalable in both cases, yielding multi-gram quantities of product with ease.

4.2.1 Raw Materials

Zeolum® zeolite molecular sieve materials were obtained from Tosoh Corporation, specifically HSZ-320NAA (faujasite structure, Na cation, SiO_2/Al_2O_3 = 5.5 mol/mol) (NaY) and HSZ-930NHA (beta structure, NH_4 cation, SiO_2/Al_2O_3 = 27 mol/mol) (NHβ). Maxsorb

MSC-30 superactivated carbon was obtained from Kansai Coke & Chemicals Company, Ltd. Activated carbon CNS-201 was obtained from A. C. Carbons Canada Inc. These materials were stored at 150°C under vacuum in a Buchi glass oven before use. Zeolite-templated carbon (ZTC) materials were prepared at HRL and Caltech by previously established methods (a representative schematic is shown in Figure 4.1).[7]

4.2.2 Caltech Experiments

At Caltech, dried zeolite (<1 wt% H_2O) and furfuryl alcohol (98%, Sigma Aldrich) were combined at room temperature under reduced pressure. In the largest batches, 3 g of dried zeolite were added to 60 mL of furfuryl alcohol and magnetically stirred for 24 h. The zeolite-furfuryl alcohol mixture was collected by vacuum filtration and washed with excess mesitylene (99.0%, Sigma Aldrich) yielding 3.5 g of a white-gray powder. The dry powder was transferred to ceramic boats and placed in N_2 flow inside a horizontal alumina tube furnace, pre-heated to 80°C. Polymerization was performed under N_2 flow at 150°C for 12 h. Temperature was increased at 2°C min^{-1} to 700°C, and gas flow was then switched to a propylene/N_2 mixture (7% propylene) for 2 h. Gas flow was switched back to pure N_2 and temperature was increased at 10°C min^{-1} to 900°C. Carbonization at 900°C was performed for 3 h. The product, referred to as Z-C, was cooled to room temperature and transferred to a PTFE beaker, yielding 2.5 g. A 3 mL aqueous solution of HF (48%, EM Industries) was added dropwise to the Z-C, stirred, and allowed to dissolve for 2 h. The aqueous solution was further diluted in a large flask to 1200 mL. The remaining solid product, ZTC, was collected by vacuum filtration and washed with water. The ZTC was dried and stored at 150°C under vacuum in a Buchi glass oven. HF treatment was repeated until no zeolite peaks remained in the x-ray diffraction (XRD) pattern, yielding 1 g of final product. By this method, two different ZTC samples were prepared: ZTC-1 from zeolite NHβ and ZTC-2 from zeolite NaY.

Experiments at Caltech lasted approximately 12 months until it was clear that limitations in control of inert atmosphere conditions during the synthetic process proved to be a barrier to achieving ultra-high surface areas. We reached ~2900 m^2 g^{-1}, but could not proceed to higher surface area or greater template fidelity. Further synthetic efforts were undertaken at HRL Laboratories, described below.

4.2.3 HRL Experiments

At HRL, 6.0 g of zeolite NaY was further dried at 450°C under vacuum for 8 h to <0.02 wt% H_2O. After cooling to room temperature, 12 mL of furfuryl alcohol (98%, Sigma Aldrich) was added by injection and the mixture was stirred under Ar atmosphere for 24 h. The zeolite-furfuryl alcohol mixture was collected via vacuum filtration and washed 4 times with 100 mL aliquots of xylenes. The washed powder was placed in a 8×8 cm shallow quartz boat and loaded into a 10 cm diameter quartz tube furnace/CVD reactor. The reactor was purged with Ar at room temperature, and was held at 80°C under Ar flow (2 L min^{-1}) for 24 h. Polymerization was performed at 150°C under Ar flow (2 L min^{-1}) for 8 h. Temperature was increased at 5°C min^{-1} to 700°C under Ar flow (2 L min^{-1}), and gas flow was then switched to a propylene/N_2 mixture (7% propylene, 3.2 L min^{-1}) for 4 h. Holding the temperature at 700°C, the reactor was purged under Ar flow (4 L min^{-1}) for 10 min. Temperature was increased to 900°C under Ar flow (2 L min^{-1}) and held for 3 h. The NaY-C product was cooled to room temperature and transferred to a

PTFE beaker where 200 mL of aqueous HF (48%, Sigma-Aldrich) were added. After 16 h, the ZTC was collected by vacuum filtration and washed 10 times with 50 mL aliquots of water. The ZTC was dried and stored at 150°C under vacuum in a Buchi glass oven, yielding 1.4 g of final product. A TGA measurement conducted in air up to 1000°C yielded a residual mass of ~2%, indicating nearly complete dissolution of the zeolite template. By this method, samples such as ZTC-3 were prepared.

By improving inert atmosphere conditions during combination of raw materials, polymerization, and carbonization, such as for ZTC-3, significant improvements in templating fidelity were observed. Careful control of inert atmosphere as well as thorough drying of the zeolite precursor was found to be critical for obtaining a product with surface area beyond 3000 $m^2 g^{-1}$.

4.3 Materials Characterization

4.3.1 Nitrogen Adsorption

Nitrogen isotherms were measured at 77 K with a BELSORP-max volumetric instrument (BEL-Japan Inc.) and surface areas were calculated using the BET method.[13] Equilibrium adsorption isotherms of N_2 at 77 K are shown in Figure 4.2. Pore-size distributions were calculated by the non-local density functional theory (NLDFT) method[14] from high-resolution data collected on a Micromeritics ASAP 2020, using a carbon slit pore model and software provided by Micromeritics. Other geometrical models were also explored, notably a unique carbon cylindrical pore model, but none showed a better fit to the data. Pore-size distributions of ZTC-3 and MSC-30 calculated

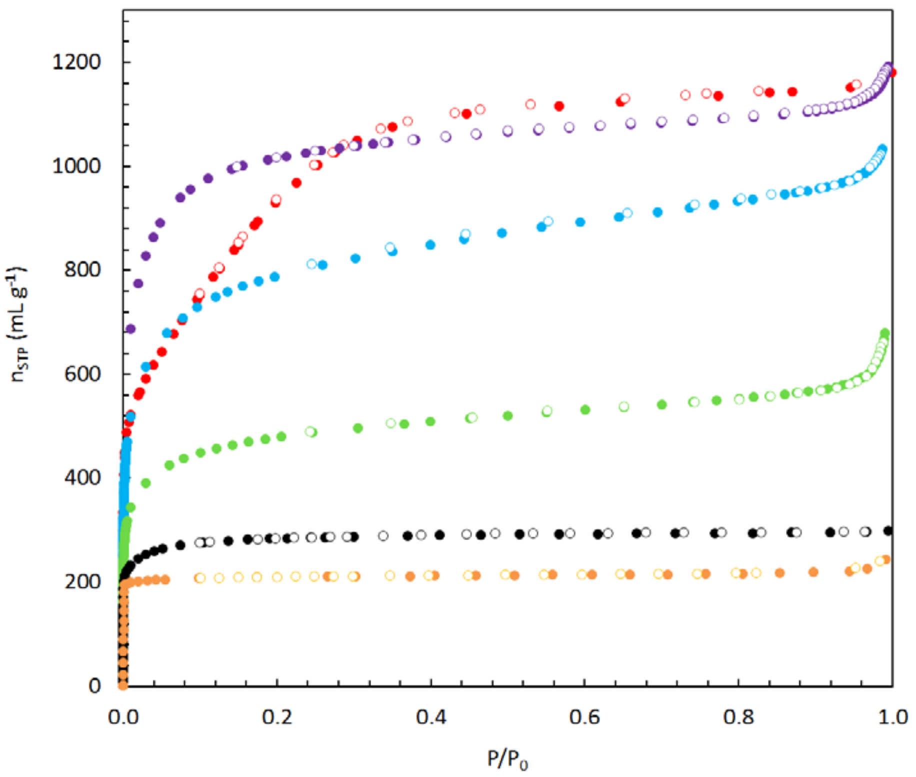

Figure 4.2. Equilibrium adsorption (closed) and desorption (open) isotherms of N_2 at 77 K on MSC-30 (red), ZTC-1 (green), ZTC-2 (blue), ZTC-3 (purple), CNS-201 (black), and zeolite NaY (orange). Uptake is expressed in units of volume of N_2 (at STP) per unit mass.

by the DFT method are shown in Figure 4.3. Distinct regularity of pore-size, centered at a width of 1.5 nm, can be seen for ZTC-3, which is consistent with other reports.[7] MSC-30 shows a broader and larger pore size distribution with significant pore volume in pores up to 3.5 nm wide. The BET surface area and Dubinin-Radushkevich (DR) micropore volume of each of the materials studied are summarized in Table 4.1. MSC-30 and CNS-201 were measured to have 3240 m^{2}g^{-1} and 1100 m^{2}g^{-1} BET surface areas, respectively. The BET surface area of MSC-30 was calculated in the region $0.0005 < P/P_0 < 0.35$, and is discussed further elsewhere[15]. All materials measured show high BET surface area and high relative uptake of N_2 in the linear region of the isotherm, among

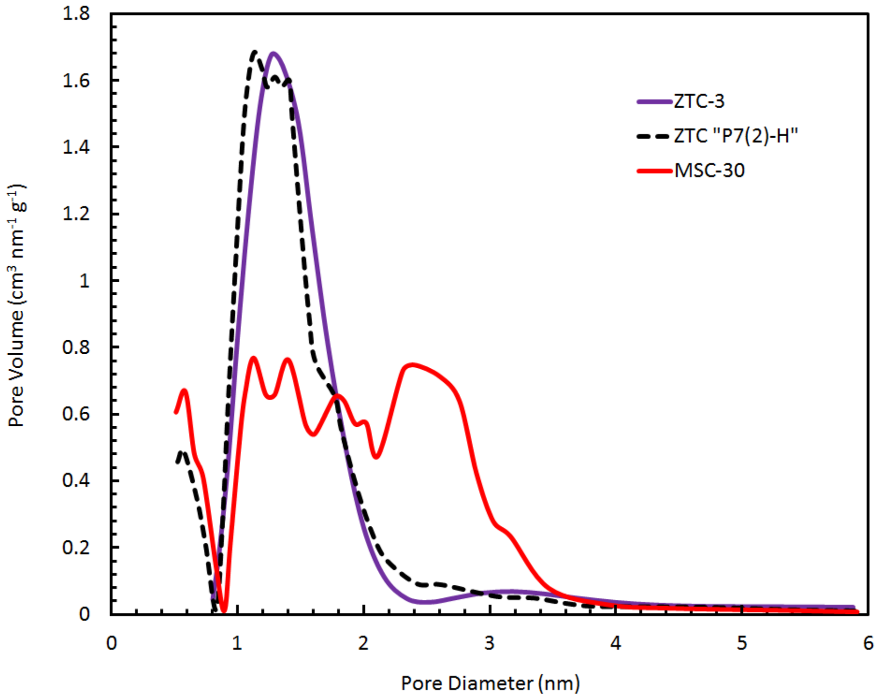

Figure 4.3. DFT pore-size distribution of ZTC-3 (purple) compared to MSC-30 (red) and ZTC "P7(2)-H" (dashed black), an equivalent reference material.[7]

Table 4.1. BET surface area (SA) and hydrogen uptake capacity reported for carbonaceous sorbent materials: CNS-201, MSC-30, and ZTCs.

Material	Density[◊] (g mL^{-1})	BET SA (m^{2}g^{-1})	H$_2$ Capacity[†] (mmol g^{-1})	High P H$_2$ Uptake[‡] (mmol g^{-1})	-ΔH$_0$ (kJ mol^{-1})
CNS-201 *	2.1	1095 ± 8	12.7	2.48	8.6
MSC-30 *	2.1	3244 ± 28	27.9	7.66	6.7
ZTC-1 *	1.9	1691 ± 21	18.5	3.99	-
ZTC-2 *	1.9	2964 ± 18	26.1	6.45	6.6
ZTC-3 *	1.8	3591 ± 60	28.6	8.27	6.5
CNS-201 [20]	2.2	1440	12.9	-	-
MSC-30 [20]	2.2	3000	26.5	-	-
MSC-30 [7]	2.1	2680	-	5.5	7.3
P7(2)-H [7]	1.9	3800	-	10.7	8

* From this study. [◊] Skeletal density measured using He at 300 K between 0-3 MPa. [†] Measured using H$_2$ at 77 K and Gibbs excess surface maximum pressure. [‡] Measured using H$_2$ at 296-303 K and 30 MPa.

the highest known for carbonaceous materials. The DR calculations were found to be susceptible to similar pitfalls as the BET method, especially for MSC-30 which shows multiple stages of different slopes in the DR curve.

4.3.2 Carbon Dioxide Adsorption

Carbon dioxide adsorption studies were carried out on early samples of ZTC, specifically ZTC-1 and ZTC-2, for comparison to MSC-30, as discussed in Appendix C.

4.3.3 Skeletal Density Measurements

Helium pycnometry measurements were performed using a standard Sieverts apparatus at pressures between 0.1-3 MPa at 298 K. Ten to thirty measurements were performed and the average skeletal densities of the materials studied are summarized in Table 4.1. ZTC-1 and ZTC-2 were measured to be 1.9 g mL^{-1}, while ZTC-3 was measured to be 1.8 g mL^{-1} , a significant difference from the activated carbons studied (both 2.1 g mL^{-1}); the standard error was ±0.06 g mL^{-1} between samples. Previous measurements of carbon materials in our laboratory gave values of 2.12 ± 0.05 g mL^{-1} over numerous different carbon types, including MSC-30. The significantly lower skeletal densities in ZTCs result in ~1 mmol g^{-1} difference in the calculated excess hydrogen uptake at 30 MPa and 298 K. This significant difference must be taken into account for uptake calculations, and seems to be unique to ZTCs as discussed in Section 4.5.1.

4.3.4 X-Ray Diffraction

X-ray diffraction (XRD) experiments were performed using a PANalytical X'Pert Pro powder diffractometer with Cu $K\alpha_{1,2}$ radiation. Diffraction patterns of ZTC-2 and ZTC-3 are shown in Figure 4.4, compared to the pure zeolite NaY precursor and the composite

NaY-C material before HF treatment. Also shown is the calculated crystal structure of the faujasite (FAU) framework. The sharp peak centered at 2θ = 6° is the (111) reflection of the cubic zeolite structure. In the final products, ZTC-2 and ZTC-3, no zeolite peaks were detected except this longest periodicity corresponding to the channel-to-channel structure of the template (14 Å), suggesting complete removal of the template from the sample; the remaining peak verifies successful templating of the zeolitic framework in the ZTC. From the width of this diffraction peak, the length scale of the zeolitic order was calculated with the Scherrer equation to be 24 nm (using the Scherrer constant K = 0.83 for spherical particles) for ZTC-3.[16] The absence of other peaks confirms the amorphous nature of C-C bonding in ZTCs, and suggests the likelihood of a turbostratic microstructure between regions of pore-to-pore periodicity.

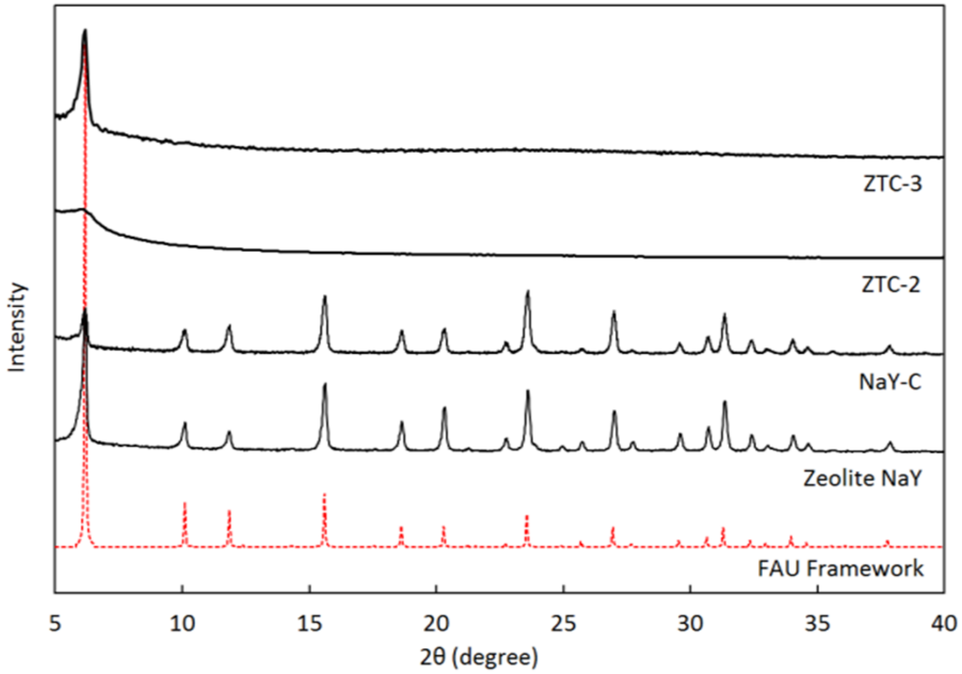

Figure 4.4. XRD patterns of final products ZTC-2 and ZTC-3, a composite zeolite-carbon intermediate product (NaY-C), pure zeolite NaY (as received), and the FAU zeolitic framework (calculated).

4.3.5 X-Ray Photoelectron Spectroscopy

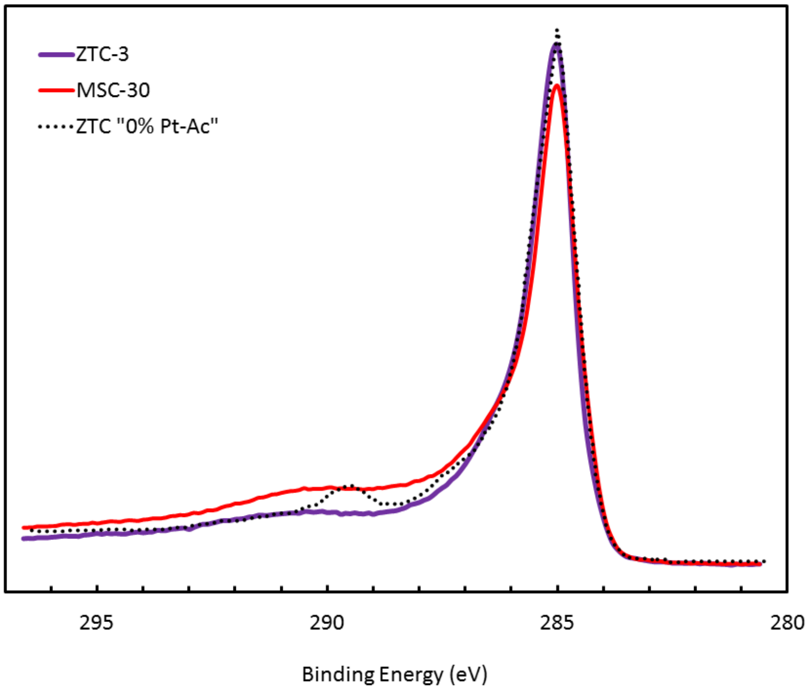

Figure 4.5. XPS data comparing ZTC-3, MSC-30, and an equivalent reference material, ZTC "0% Pt-Ac.".[16]

X-ray photoelectron spectroscopy (XPS) was performed to compare ZTCs to MSC-30, but no appreciable difference was found (see Figure 4.5). XPS studies were performed on a Kratos AXIS Ultra DLD spectrometer with a monochromatic Al-Kα source operating at 150 W, with a 20 eV pass energy, and 0.1 eV step (after brief survey spectra were collected). The binding energy was corrected to the most intense peak, which is from sp^2 hybridized carbon, at 285.0 eV. The intensity was not rescaled since identical instrumental conditions were used across all samples. For peak fitting analysis, a Shirley-type background was subtracted and 8 component peaks were fitted, following a previously reported procedure.[17] An example of peak fits is shown in Figure 4.6. The results are summarized in Table 4.2, indicating 18% and 19% sp^3 hybridized carbon in ZTC-3 and MSC-30, respectively.

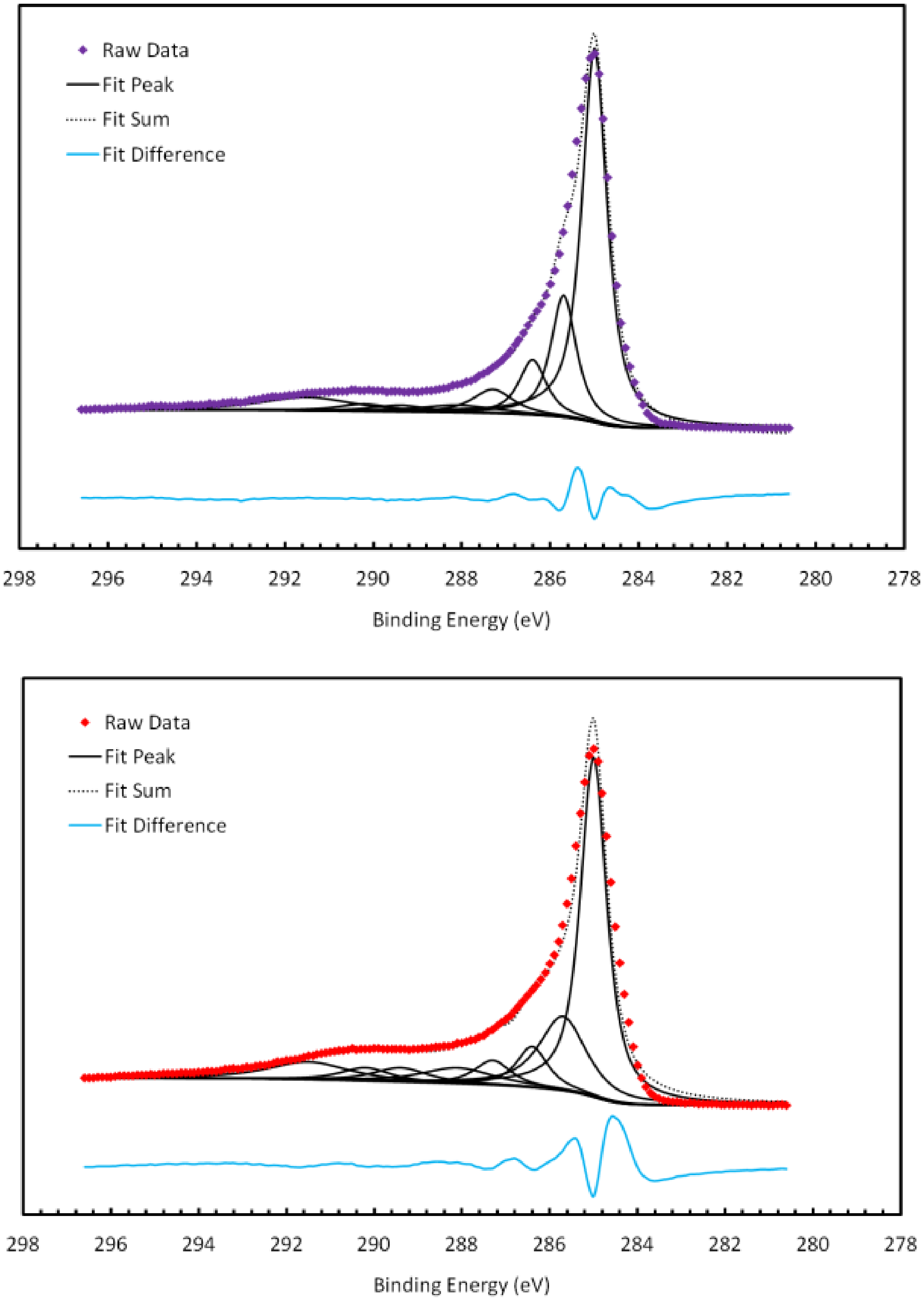

Figure 4.6. XPS analyses for the carbon 1s regions in ZTC-3 (top) and MSC-30 (bottom).

Table 4.2. Summary of the XPS analysis results for ZTC-3 and MSC-30.

	Component Fraction (at%)							
Peak Position (eV)	285.0	285.7	286.4	287.3	288.1	289.4	290.2	291.5
Component	C-C sp^2	C-C sp^3	C-OR	C-O-C	C=O	COOR	-	-
ZTC-3	53.4	18.0	8.6	6.0	1.1	4.2	1.0	7.7
MSC-30	48.0	18.8	6.8	4.8	6.1	4.2	3.6	7.7

4.3.6 Electron Microscopy

SEM studies were performed on a Hitachi S-4800 instrument operated at 4.0 keV. Samples were prepared for SEM by dispersing in isopropanol on a holey carbon grid. Evidence can be seen of the superficial likeness between particles of ZTC and the zeolite template from which they were synthesized (shown in Figure 4.7), similar to that reported by Ma et al.[18]

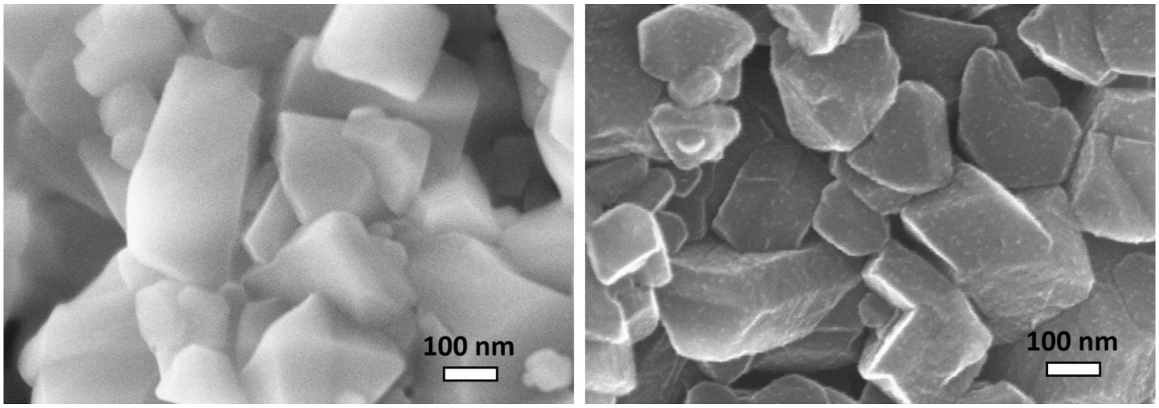

Figure 4.7. SEM micrographs of zeolite precursor (left) and ZTC product (right), showing similar particle size and shape.

TEM studies were performed on a FEI Tecnai F20 instrument operated at 200 keV. Samples were prepared for TEM by dispersing a finely ground mixture of ZTC and isopropanol on a holey carbon grid. Low magnification TEM studies were consistent with the SEM data. A high magnification micrograph of a thin region of ZTC-3 is shown in

Figure 4.8, with an inset showing the Fourier transform of the image. The spots in the transformed image confirm the periodicity of the porous structure. The pore-to-pore spacing of 1.0 nm is consistent with that calculated from DFT treatment of the N_2 adsorption isotherms at 77 K (see Figure 4.3), and with data reported by Ma et al.[18]

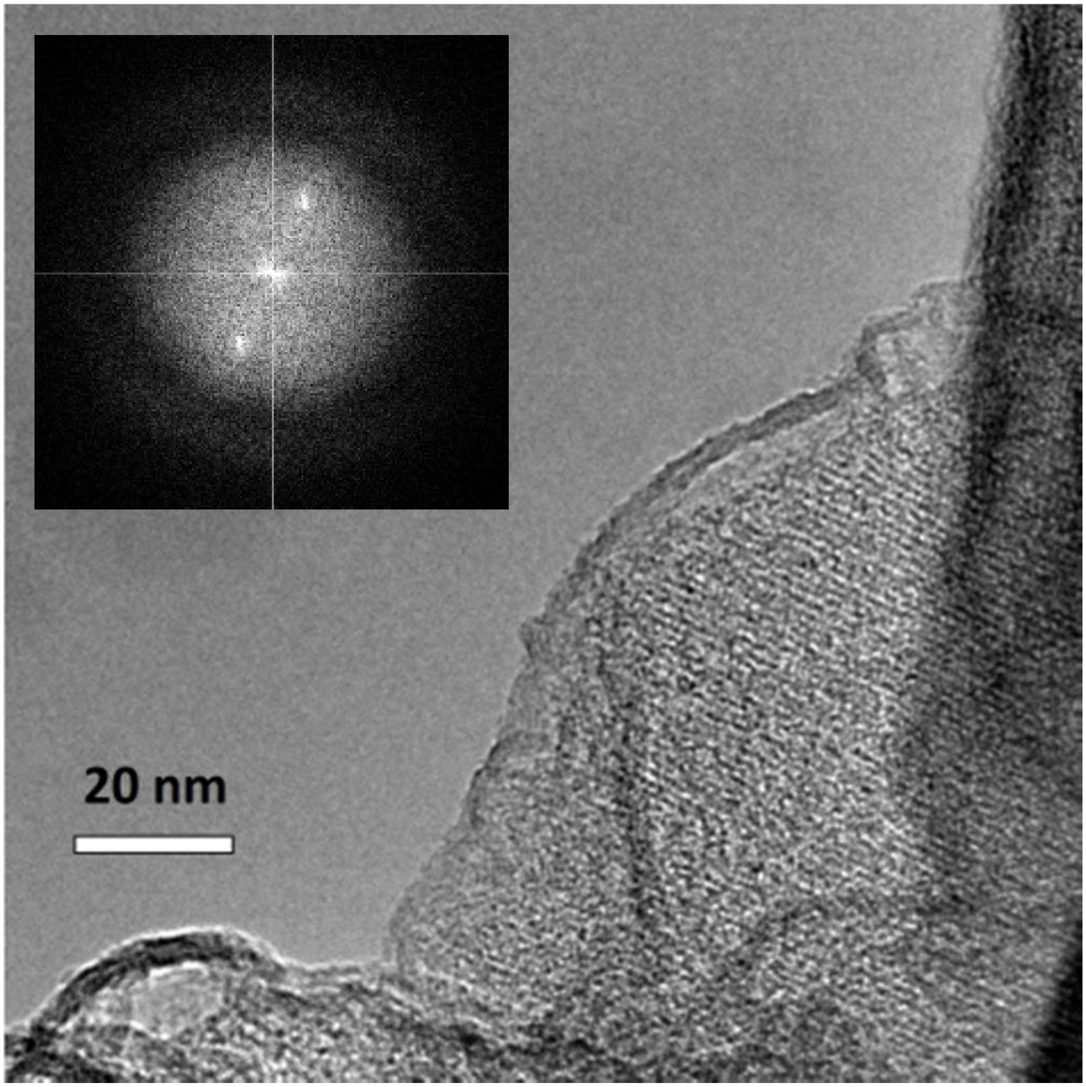

Figure 4.8. TEM micrograph of ZTC-3 showing pore-to-pore periodicity of 1.0 nm, and the Fourier transform of the image (inset).

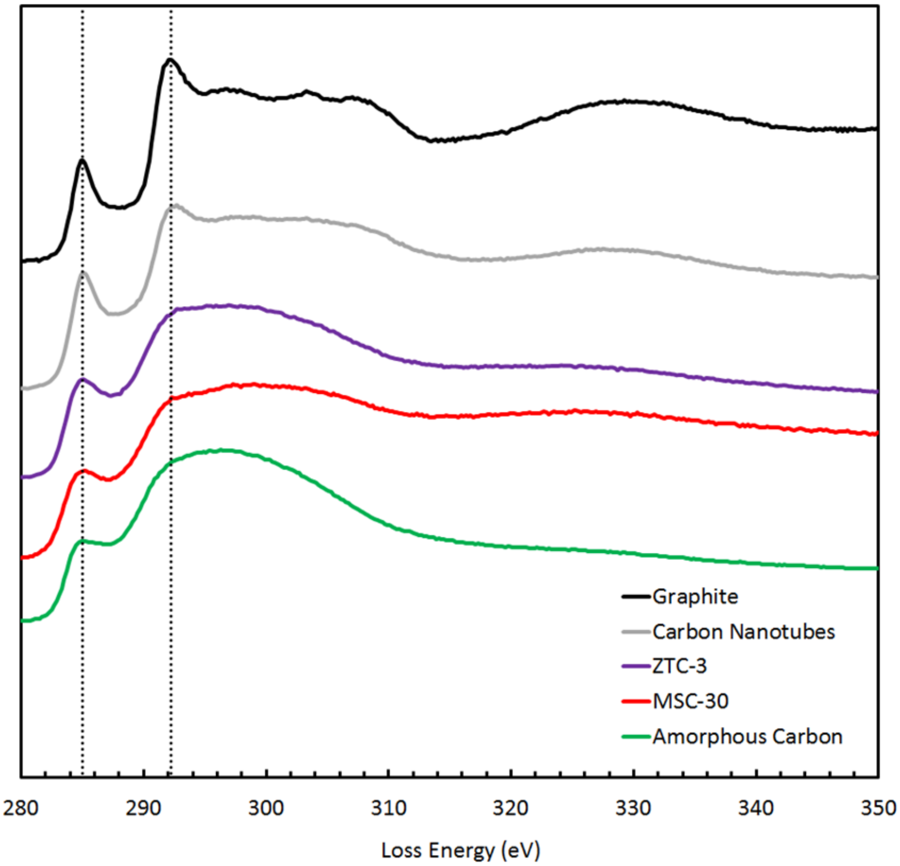

Figure 4.9. EELS spectra showing the carbon 1s edge in ZTC-3 compared to MSC-30, graphite, carbon nanotubes, and the amorphous holey carbon grid.

4.3.7 Electron Energy-Loss Spectroscopy

Electron energy-loss spectroscopy (EELS) was performed to compare ZTCs to MSC-30 and other carbon materials, shown in Figure 4.9. EELS measurements were performed on a FEI Tecnai F20 instrument operated at 200 keV and equipped with a Gatan Imaging Filter system. To acquire these spectra, the aperture size was 0.6 mm, the dispersion was 0.2 eV pixel^{-1}, and the energy shift was 175 eV. Samples were prepared by dispersing a finely ground mixture of sample material and isopropanol on a holey carbon grid. The pre-edge peak was calibrated to 285.0 eV in all samples, a power-law background was subtracted, and the signal intensity was normalized to the same value at high loss. The ratio of the areas of the pre-edge peak to the main carbon 1s edge (>289 eV) was used to determine the relative content of sp^2 and sp^3 hybridized carbon (see Figure 4.10). This study also shows only a small difference in the amount of sp^2 and sp^3 hybridized carbon between ZTC-3 and MSC-30: approximately 18% and 16% sp^3 content, respectively.

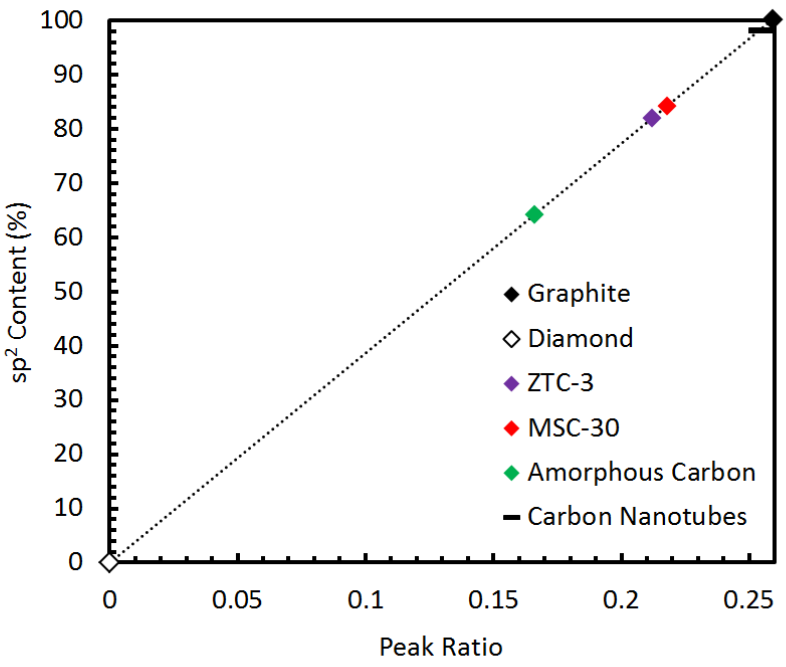

	◆	◇	🟪	🟥	🟩	▬
P1 Area = $I_{\pi*}$	1.54	0	1.96	1.95	1.55	2.08
P2 Area = $I_{\sigma*}$	4.41	1	7.30	6.97	7.75	6.09
P1/P2	0.35	0	0.27	0.28	0.20	0.34
$I_{\pi*}/(I_{\pi*}+I_{\sigma*})$	0.26	0	0.21	0.22	0.17	0.25
Normalized	1	0	0.82	0.84	0.64	0.98
sp^2 Content (%)	100	0	81.8	84.2	64.2	98.3

Figure 4.10. Summary of sp^2 content in carbon materials studied by EELS, based on the integrated peak areas of the 1s→π* peak at ~285 eV to the 1s→σ* peak at ~292 eV, and fit to a calibration curve established by graphite and diamond.

4.3.8 Solid-State Nuclear Magnetic Resonance

Solid-state ^{13}C NMR experiments were performed on ZTC-3 and MSC-30 using a Bruker DSX-500 spectrometer equipped with a Bruker 4 mm MAS probe (see Figure 4.11). The sample spinning rates were 12 kHz and 5 kHz for MAS and CPMAS, respectively, performed at room temperature under dry nitrogen gas. CPMAS measurements were performed with a RF field of 62.5 kHz during the CP contact period (0.1 ms). The chemical shifts are given in parts per million (ppm) externally referenced to tetramethylsilane. No significant sp^3 hybridized carbon (10-50 ppm region) in either ZTC-3 or MSC-30 was detected, consistent with previous measurements.[19]

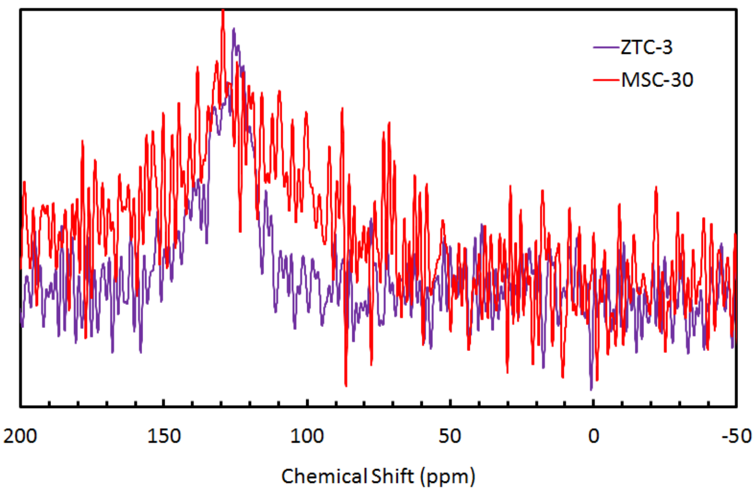

Figure 4.11. Solid-state ^{13}C NMR (MAS) spectra of ZTC-3 and MSC-30.

A cross-polarization ^{13}C MAS (CPMAS) study was also carried out, and compared to the MAS data, shown in Figure 4.12. The results are consistent with a previous report.[19] A peak fitting analysis was performed to determine the protonated content of carbon in the sp^2 peak. By deconvolution of the main peak into 3 components, it is calculated that ~89% of carbon ZTC-3 is protonated, from the contribution of the fit peak centered at

138 ppm. While an overestimate, this is consistent with results confirming high H content in ZTCs by elemental analysis experiments (see Section 4.5.1).

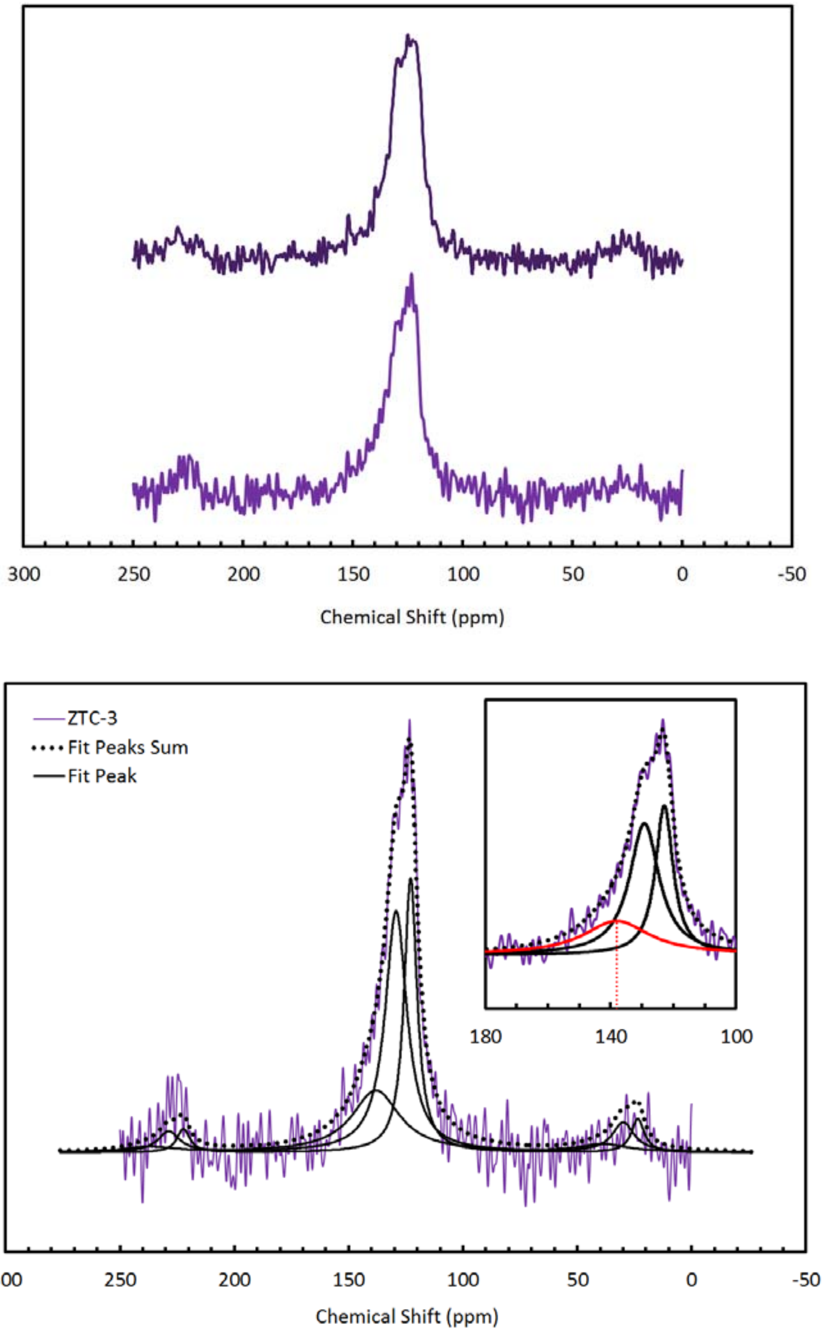

Figure 4.12. Solid-state ^{13}C MAS NMR spectrum of ZTC-3, fitted to three peaks (centered at 130, 136, and 138 ppm). The peak at 138 ppm was not present in CPMAS spectra, and is attributed to non-protonated sp^2 hybridized carbon, accounting for ~11% of the area of the total signal.

4.4 Hydrogen Adsorption

4.4.1 Standard-Pressure Experiments

Hydrogen adsorption isotherms were measured at 77 and 87 K from 0-7 MPa on the Sieverts I apparatus. Temperature baths of liquid nitrogen (77 K) and liquid argon (87 K) were continually filled throughout experiments to maintain low temperature conditions in the sample cell if necessary. The system was leak checked up to 7 MPa and showed a maximum leak rate of 6.0×10^{-7} mol h^{-1} of H_2. If fitted to an exponential decay function (see Equation 3.1) where k is the leak rate, this corresponds to a maximum leak of k ~ 10^{-9} s^{-1} which is well within the acceptable limit for accurate measurements.[20] During measurements, the system was not returned to vacuum between steps, and the measured hydrogen uptake was cumulative.

4.4.2 High-Pressure Experiments

Hydrogen adsorption isotherms at 298 K were measured up to 30 MPa on the Sieverts II apparatus. The temperature of the sample was not controlled, but remained within ±0.3 K. High pressures were achieved by gas densification in a coil submerged in a liquid nitrogen bath that was removed to allow the coil to return to ambient temperature. Hydrogen uptake was determined in cumulative steps, as in Section 3.4.1. The system was leak tested up to 45 MPa and showed a maximum leak rate of 2.2×10^{-7} mol h^{-1} of H_2. This corresponds to a maximum leak of k ~ 10^{-8} s^{-1}. Hydrogen uptake isotherms measured on MSC-30 using Sieverts II were compared to isotherms collected on Sieverts I and the gravimetric balance at EMPA, and were consistent from 0-10 MPa.

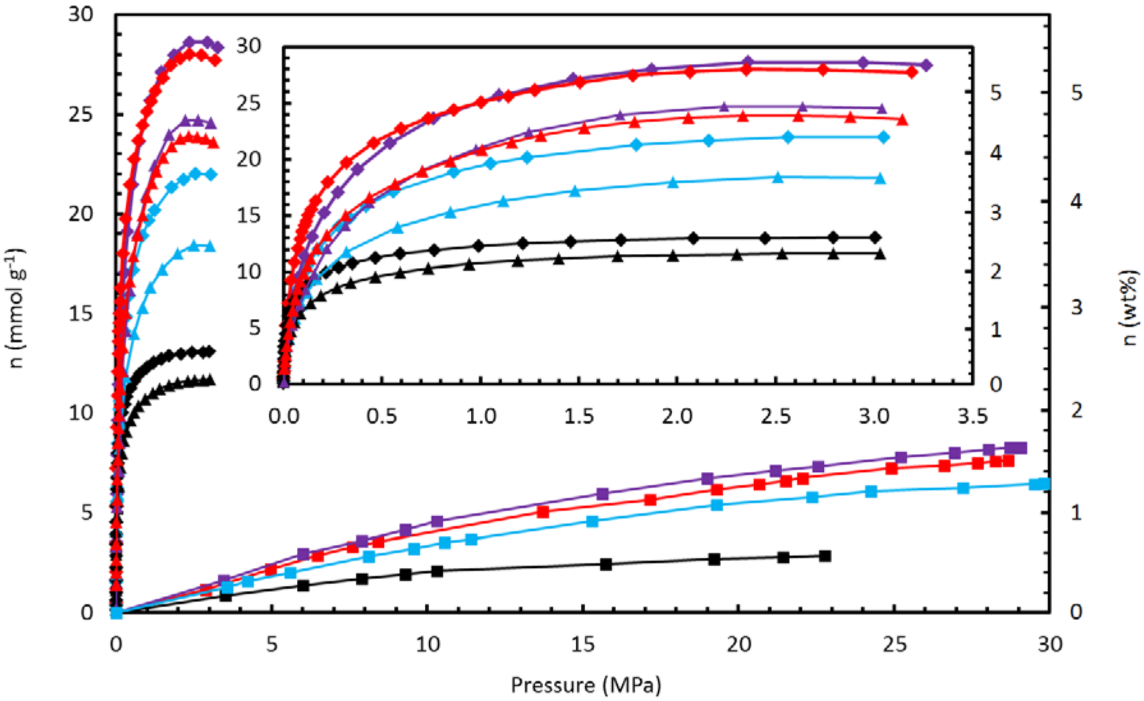

Figure 4.13. Equilibrium adsorption isotherms of hydrogen on MSC-30 (red), ZTC-2 (blue), ZTC-3 (purple), and CNS-201 (black) at 77 K (diamond), 87 K (triangle), and 298 K (square) between 0-30 MPa (inset shows detail between 0-3.5 MPa).

4.4.3 Hydrogen Adsorption Results

The complete set of equilibrium adsorption isotherms of hydrogen on CNS-201, MSC-30, ZTC-2, and ZTC-3 is shown in Figure 4.13. Hydrogen adsorption at all temperatures and pressures was fully reversible in all materials studied after numerous cycles. The Gibbs surface excess maximum hydrogen capacities of the materials are summarized in Table 4.1. The highest measured was for ZTC-3: 28.6 mmol g^{-1} (5.5 wt%) at 2.4 MPa. Maximum uptake was higher in ZTC-3 than MSC-30 despite a more gradual initial increase at low pressure.

Equilibrium adsorption isotherms of H_2 on ZTCs, MSC-30, and CNS-201 were measured up to 30 MPa at room temperature, and are shown in Figure 4.14 (the same data as in Figure 4.13, isolated for clarity). Excess hydrogen capacities of the materials were calculated by extrapolation of the data to 30 MPa and are summarized in Table 4.1. The highest measured was for ZTC-3: 8.3 mmol g^{-1} (1.6 wt%) at 30 MPa and 298 K.

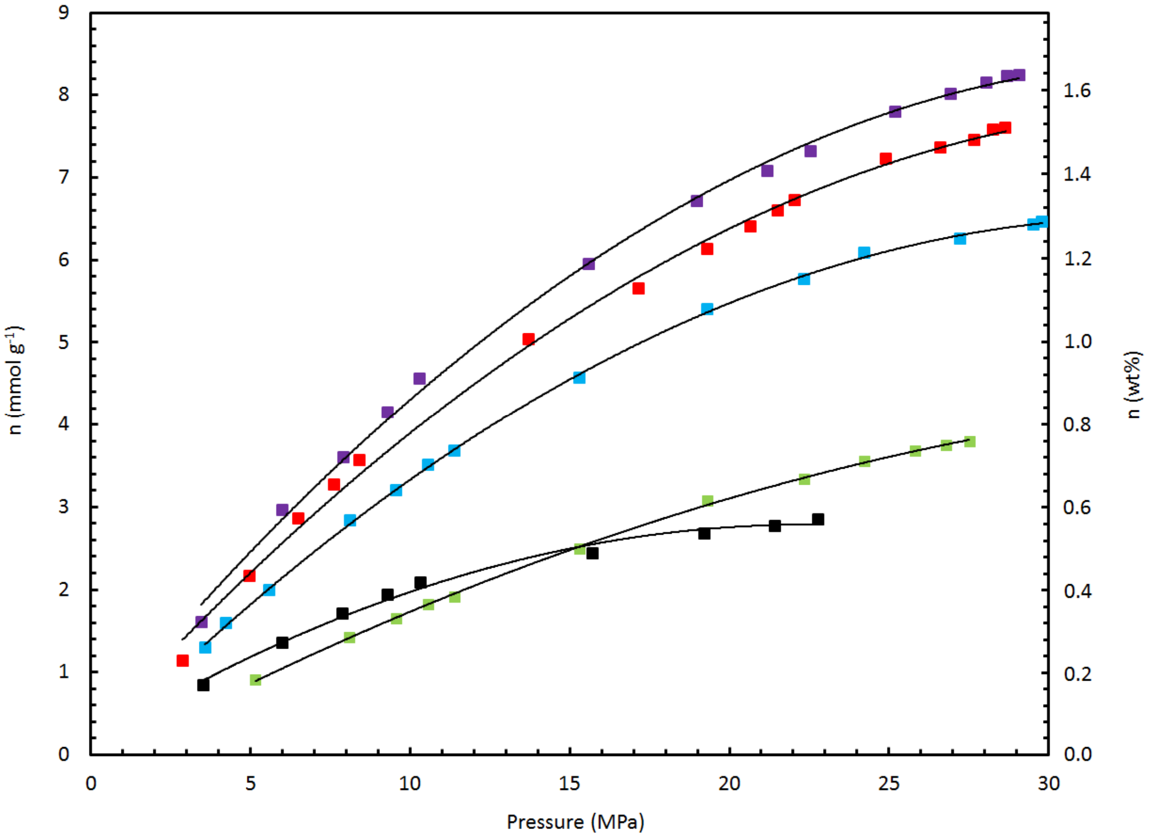

Figure 4.14. Equilibrium adsorption isotherms of H_2 on MSC-30 (red), ZTC-1 (green), ZTC-2 (blue), ZTC-3 (purple), and CNS-201 (black) at 298 K between 0-30 MPa.

Verification of the calibration of our high-pressure volumetric apparatus was by measurements of commercial materials MSC-30 and CNS-201. However, comparison of standard materials to references was found to be reliable only in some instances. The superactivated carbon MSC-30, a material processed similarly to Anderson AX-21, is reported to have a BET surface area ranging from 2600-3400 m^2 g^{-1}.[2, 7, 21-23] This variation is not only due to differences in the analysis of the N_2 adsorption isotherms at

77 K, but is also reflected in differences in hydrogen adsorption isotherms at temperatures from 77-298 K, implying that different batches of MSC-30 have different properties. Hydrogen capacities of MSC-30 at 298 K range from 3-4 mmol g^{-1} (0.6-0.8 wt%) at 10 MPa; in this report, it was measured to be 3.9 mmol g^{-1} which is consistent with the upper end of this range. Hydrogen uptake in CNS-201 was 2.0 mmol g^{-1}, compared to a reference value of 2.1 mmol g^{-1}.[21]

4.4.4 Enthalpy of Adsorption

The equilibrium excess hydrogen adsorption data for ZTC-3, MSC-30, and CNS-201 were fitted in two ways: using a typical "isoexcess" model-independent virial-type fitting equation (to 3rd order terms), and using a generalized double-Langmuir fitting equation which allows the determination of the absolute adsorption quantity. The enthalpy of adsorption was calculated by the isoexcess and isosteric method, respectively (see Sections 2.4-5).

Plots of the isoexcess enthalpy of adsorption of hydrogen on CNS-201, MSC-30, ZTC-2 and ZTC-3 are shown in Figure 4.15. The isosteric enthalpy of adsorption calculated using the real gas density of hydrogen on CNS-201, MSC-30, and ZTC-3 is shown in Figure 4.16. In both cases, the calculations were performed by fitting the data from the entire range of temperature between 77-298 K. For the isoexcess method, only an average enthalpy was accessible while the isosteric enthalpy could be calculated at arbitrary temperatures within the temperature range measured. The average Henry's law values, $-\Delta H_0$, for the materials studied are summarized in Table 4.1.

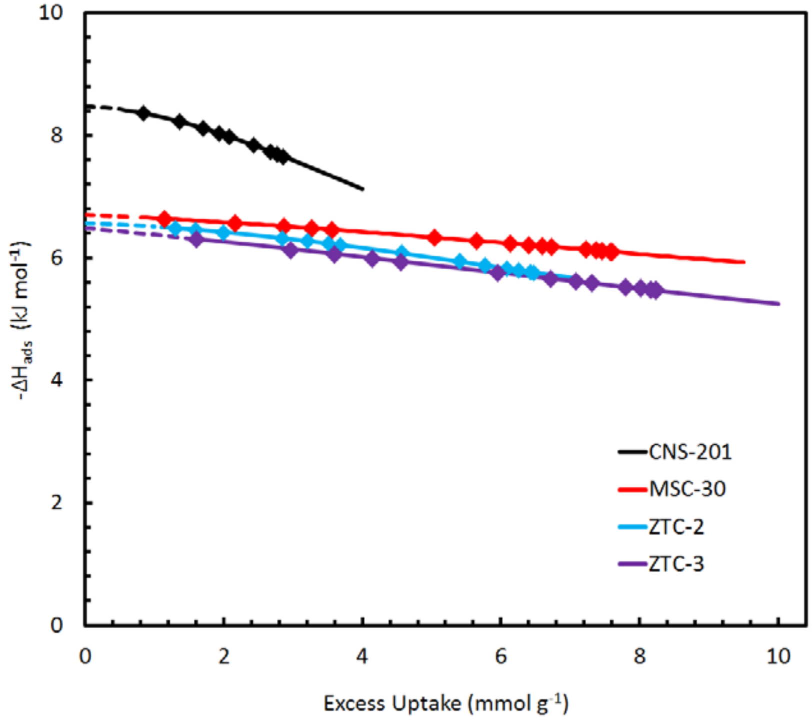

Figure 4.15. Average isoexcess enthalpy of adsorption of hydrogen on CNS-201 (black), MSC-30 (red), and ZTC-3 (purple) as a function of excess uptake between 77-298 K.

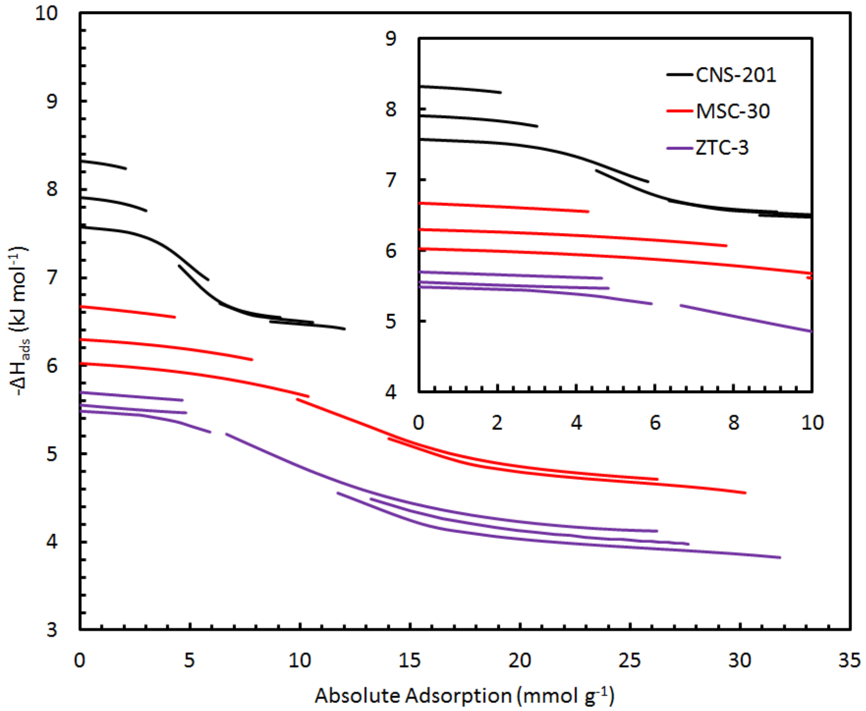

Figure 4.16. Isosteric enthalpy of adsorption of hydrogen on CNS-201 (black), MSC-30 (red), and ZTC-3 (purple) as a function of absolute uptake, at temperatures from 77-298 K.

Similar results are found using both methods due to the near-ideal properties of hydrogen in the temperature and pressure range measured. The highest value reported is for CNS-201 which is known to have an exceptionally high binding energy for hydrogen.[24] It decreases substantially as uptake increases, which is also reflected in the shape of the hydrogen uptake curves for CNS-201 at all temperatures. The adsorption enthalpy calculated for ZTCs and MSC-30 decreases only slightly and is relatively constant as uptake increases; the continued increase in uptake at 30 MPa compared to CNS-201 can be attributed to this characteristic of the higher surface area materials.

4.5 Discussion

The addition of sorbent material to a storage tank has two consequences: the volume available for gaseous storage is decreased (by the material's skeletal density) and the surface available for van der Waals interactions is increased (by the material's specific surface area). With enthalpy of adsorption in the range of 4-9 kJ mol^{-1}, as is observed for carbon materials, careful measurements of sample density and surface area are critical for characterizing sorption capacity and can be used together to readily predict material performance in the temperature and pressure conditions studied: 77-298 K and 0-30 MPa.

4.5.1 Skeletal Density

Skeletal density is the only material specific variable required, and therefore the most important variable in accurate determination of excess hydrogen uptake in adsorption measurements. Carbonaceous materials often have a similar skeletal density to graphite, 2.1-2.2 g mL^{-1}.[21] However, skeletal densities in ZTCs are significantly lower, 1.8 g mL^{-1}. This indicates a less graphitic nature of ZTCs, but is not easily explained since ZTCs are predominantly sp^2 carbon.[17, 18] Distortions such as bond stretching or vacancy defects which could alter the ratio of sp^2 to sp^3 bonding of carbon atoms would have to be large to account for this difference. However, the fractions of sp^2 and sp^3 bonding were found to be similar through auxiliary measurements by x-ray photoelectron spectroscopy (XPS), electron energy-loss spectroscopy (EELS), and solid-state ^{13}C NMR.

One explanation of the significantly lower skeletal density of ZTCs can be given by recent results from elemental analysis experiments. Elemental composition (CHN) of MSC-30 and ZTC-3 was determined by triplicate combustion experiments, using the Dumas method.[25] Samples were prepared by degassing at 250°C and sealed in foil packets in an argon glovebox with < 1 ppm H_2O, a critical step for obtaining an accurate estimate of the H content since any adsorbed H_2O would contribute to detected H. Average hydrogen content in ZTC-3 was 2.4 wt% H, approximately twice that in MSC-30: 1.2 wt% H. If each atomic site where carbon is substituted for hydrogen retains its original skeletal volume, the difference in skeletal density would be 11%, a decrease from 2.1 to 1.9 g mL^{-1}. Additional decrease in skeletal density could be due to the presence of hanging C-H groups which have a larger atomic volume than a pair of sp^2 hybridized carbon atoms. This approximation gives a representative figure for the significance of increased H content to the skeletal density, an effect that is large enough to account for the difference between MSC-30 and ZTC-3.

4.5.2 Surface Area

Hydrogen uptake at 77 K and 298 K is generally proportional to surface area in the materials studied, as shown in Figure 4.17. The relationship for ZTCs at 77 K is ~9 mmol g^{-1} (1.8 wt%) Gibbs surface excess maximum hydrogen capacity per 1000 m^2 g^{-1} BET surface area, the same as for other carbonaceous materials.[3] This corresponds to 5.4 molecules of H_2 per nm^2 of BET surface area. The relationship for ZTCs at 30 MPa and 298 K is 2.3 mmol g^{-1} (0.46 wt%) excess hydrogen uptake per 1000 m^2 g^{-1} BET surface area, the same as for other carbonaceous materials in this study. Importantly, this result is contrary to a previous result[7] which reports higher uptake in ZTCs at 303 K: 2.8 mmol g^{-1} (0.55 wt%) excess hydrogen uptake per 1000 m^2 g^{-1} BET surface area in “P7(2)-H,” compared to 2.0 mmol g^{-1} (0.41 wt%) per 1000 m^2 g^{-1} in MSC-30. In this previous report, a 100% increase in uptake was measured for ZTCs compared to MSC-30, and it could not be explained by surface area. Compared to the results in this study, the measurement of uptake in ZTC “P7(2)-H” was erroneously high, while uptake in MSC-30 was underestimated, contributing to a large apparent enhancement in hydrogen capacity of ZTC compared to MSC-30.

While ZTCs measured in the present study show increased uptake compared to MSC-30, this was consistent with their larger specific surface area. These relationships are critically dependent on the accurate and consistent determination of specific surface area of the sorbent material and the assumptions inherent to BET theory. The known shortcomings of this method for microporous materials are thought to be approximately equal in the materials studied. However, extreme care must still be taken in analysis of

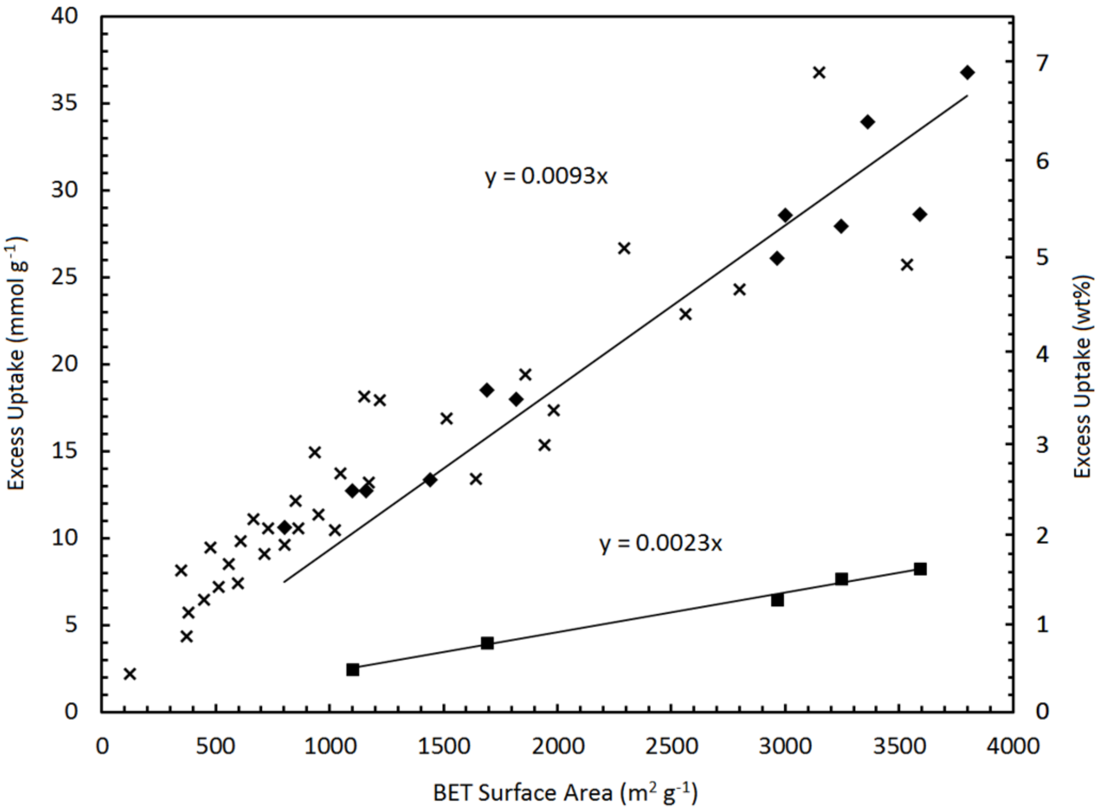

Figure 4.17. Equilibrium excess adsorption uptake of hydrogen as a function of BET surface area at 77 K (Gibbs excess surface maximum capacity: diamond) and 298 K (at 30 MPa: square). An × indicates a reported value from the literature, at 77 K.

the nitrogen isotherms at 77 K; assumption of a standard pressure range over which to fit the BET equation is not appropriate. The region from low pressure up to the knee of the isotherm (“point B” for a type II isotherm) must be included as this pressure range is different for each material. For MSC-30, the calculation is especially sensitive to the range chosen because the knee is rounded and there are two nearly linear regions in the isotherm (type IV like character). Even for classic type II isotherms, BET surface area is often miscalculated: in “CB850h,” a ZTC which was reported to have a maximum excess hydrogen capacity of 8.33 wt% at 77K, the BET surface area is calculated to be 3150 m^2 g^{-1}.[26] This value would represent an extreme outlier on a plot of hydrogen capacity at

77K as a function of surface area; however, our analysis of the reported N_2 isotherm data gives a BET surface area of 3800 m^2 g^{-1}, much closer to the expected value for such a high capacity sorbent. Similarly, “P7(2)-H” was reported to have a BET surface area of 3800 (while our analysis yields a value of 3538 ± 50) m^2 g^{-1}.[7] Another method of ranking similar sorbents of the same material class is by comparing the nitrogen uptake capacity at 77 K and an intermediate pressure, say P/P_0 = 0.5. This analysis also shows “CB850h” to be among the highest performance sorbent materials and explains the large excess hydrogen capacity at 77 K. ZTC-3 was found to be nearly identical to “P7(2)-H” in this comparison and explains the similar surface area when a consistent calculation method is used.

4.5.3 Enthalpy of Adsorption

The similarity of isoexcess enthalpies of adsorption between ZTCs and MSC-30 in Figures 4.15 and 4.16 implies that there are no significant differences in the dispersion forces responsible for hydrogen physisorption. The high-pressure data at 298 K allows the unique contribution of high temperature data to the calculation of isoexcess enthalpy of adsorption. However, dispersion forces are known to have a significant temperature dependence.[27, 28] For instance, the heat of adsorption of hydrogen on MOF-5 is reported to increase by up to 1 kJ mol^{-1} between cryogenic and room temperatures.[27] Therefore, the values given in Table 4.1 are to be understood as averages over the whole temperature range for the given material. Indeed, when a more sophisticated method was used to determine isosteric enthalpy of adsorption, the double-Langmuir fitted results shown in Figure 4.16, a similar temperature dependence of the enthalpy was calculated between all materials: 2-4 J mol^{-1} K^{-1}. It is important to note that this analysis method works best on data sets with numerous isotherms in a close temperature range, preferably spaced by 10-20 K. The three temperatures collected in this study were much further apart, and the fits were difficult to optimize; the data plotted in a narrow range for each temperature (as in Figure 4.16) was the best representation of the dependence of enthalpy with uptake.

The hydrogen uptake character in ZTCs at 77 K, especially ZTC-3, is slightly different from MSC-30 because the uptake is lower between 0-1.0 MPa, but exceeds MSC-30 between 1.0-2.4 MPa. For effective hydrogen delivery by a sorbent material between two finite pressures, $P_f - P_i$, it is favorable to have an excess uptake slope that is gradual below P_f and steep in the cycled region of uptake/delivery; the quantity of hydrogen delivered is the difference between the amount in the initial (fully charged) state at P_i and the final (considered "empty") state at P_f. For delivery to a fuel cell, P_f is often taken to be 0.3 MPa.[29] Therefore, ZTCs used for this purpose at 77 K exhibit higher hydrogen delivery than MSC-30 by 15% when cycled between 0.3-2.4 MPa.

4.6 Conclusions

Equilibrium hydrogen uptake capacities of ZTCs at room temperature are among the highest of known physisorbent materials due to their large specific surface area. Hydrogen adsorption capacity in ZTCs is approximately proportional to surface area at 298 K between 0-30 MPa, and is consistent with a large variety of carbonaceous materials, including activated carbons, carbon fibers, graphite, aerogels, and nanotubes.

That is, a "Chahine's rule" type of trend is observed at room temperature and fixed pressure for carbon-based materials, including ZTCs. This trend is found to be 2.3 mmol g^{-1} (0.46 wt%) excess hydrogen uptake per 1000 m^2 g^{-1} BET surface area at 298K and 30 MPa. ZTCs were found to have an isoexcess enthalpy of adsorption comparable to MSC-30 when measured between 77-298 K: 6.5 kJ mol^{-1} in the Henry's law limit. This implies that there are no significant differences in the dispersion forces responsible for hydrogen physisorption in ZTCs compared to MSC-30. Unlike other carbons, ZTCs were measured to have significantly lower skeletal density; this has the effect of increasing calculated uptake and straightening the uptake curve with increasing pressure. This is beneficial for gravimetric hydrogen delivery by ZTCs during cycling between two finite pressures in an engineering application, especially at 77 K.

4.7 References

(1) J. Purewal, J. Keith, C. Ahn, B. Fultz, C. Brown, and M. Tyagi, 'Adsorption and melting of hydrogen in potassium-intercalated graphite', *Phys. Rev. B,* **79** (2009).

(2) E. Poirier, R. Chahine, and T. K. Bose, 'Hydrogen adsorption in carbon nanostructures', *Int. J. Hydrogen Energ.,* **26**, 831-835 (2001).

(3) B. Panella, M. Hirscher, and S. Roth, 'Hydrogen adsorption in different carbon nanostructures', *Carbon,* **43**, 2209-2214 (2005).

(4) R. Ströbel, J. Garche, P. T. Moseley, L. Jörissen, and G. Wolf, 'Hydrogen storage by carbon materials', *J. Power Sources,* **159**, 781-801 (2006).

(5) T. Kyotani, 'Control of pore structure in carbon', *Carbon,* **38**, 269-286 (2000).

(6) T. Kyotani, T. Nagai, S. Inoue, and A. Tomita, 'Formation of new type of porous carbon by carbonization in zeolite nanochannels', *Chem. Mater.,* **9**, 609-615 (1997).

(7) H. Nishihara, P. X. Hou, L. X. Li, M. Ito, M. Uchiyama, T. Kaburagi, A. Ikura, J. Katamura, T. Kawarada, K. Mizuuchi, and T. Kyotani, 'High-pressure hydrogen storage in zeolite-templated carbon', *J. Phys. Chem. C,* **113**, 3189-3196 (2009).

(8) M. A. de la Casa-Lillo, F. Lamari-Darkrim, D. Cazorla-Amorós, and A. Linares-Solano, 'Hydrogen storage in activated carbons and activated carbon fibers', *J. Phys. Chem. B,* **106**, 10930-10934 (2002).

(9) B. Liu, H. Shioyama, T. Akita, and Q. Xu, 'Metal-organic framework as a template for porous carbon synthesis', *J. Am. Chem. Soc.,* **130**, 5390-5391 (2008).

(10) B. Liu, H. Shioyama, H. Jiang, X. Zhang, and Q. Xu, 'Metal-organic framework (MOF) as a template for syntheses of nanoporous carbons as electrode materials for supercapacitors', *Carbon,* **48**, 456-463 (2010).

(11) H.-L. Jiang, B. Liu, Y. Q. Lan, K. Kuratani, T. Akita, H. Shioyama, F. Zong, and Q. Xu, 'From metal-organic framework to nanoporous carbon: toward a very high surface area and hydrogen uptake', *J. Am. Chem. Soc.,* **133**, 11854-11857 (2011).

(12) H. Nishihara and T. Kyotani, 'Templated nanocarbons for energy storage', *Adv. Mater.,* **24**, 4473-4498 (2012).

(13) S. J. Gregg and K. S. W. Sing, *Adsorption, surface area, and porosity*, Academic Press, London (1982).

(14) P. Tarazona, U. M. B. Marconi, and R. Evans, 'Phase equilibria of fluid interfaces and confined fluids', *Mol. Phys.,* **60**, 573-595 (1987).

(15) N. P. Stadie, J. J. Vajo, R. W. Cumberland, A. A. Wilson, C. C. Ahn, and B. Fultz, 'Zeolite-templated carbon materials for high-pressure hydrogen storage', *Langmuir,* **28**, 10057-10063 (2012).

(16) J. I. Langford and A. J. C. Wilson, 'Scherrer after sixty years: a survey and some new results in the determination of crystallite size', *J. Appl. Crystallogr.,* **11**, 102-113 (1978).

(17) Y. Yang, C. M. Brown, C. Zhao, A. L. Chaffee, B. Nick, D. Zhao, P. A. Webley, J. Schalch, J. M. Simmons, Y. Liu, J.-H. Her, C. E. Buckley, and D. A. Sheppard, 'Micro-channel development and hydrogen adsorption properties in templated microporous carbons containing platinum nanoparticles', *Carbon,* **49**, 1305-1317 (2011).

(18) Z. Ma, T. Kyotani, and A. Tomita, 'Synthesis methods for preparing microporous carbons with a structural regularity of zeolite Y', *Carbon,* **40**, 2367-2374 (2002).

(19) Z. Ma, T. Kyotani, Z. Liu, O. Terasaki, and A. Tomita, 'Very high surface area microporous carbon with a three-dimensional nano-array structure: synthesis and its molecular structure', *Chem. Mater.,* **13**, 4413-4415 (2001).

(20) L. Schlapbach, 'Hydrogen as a fuel and its storage for mobility and transport', *MRS Bull.,* **27**, 675-679 (2002).

(21) M.-A. Richard, D. Cossement, P.-A. Chandonia, R. Chahine, D. Mori, and K. Hirose, 'Preliminary evaluation of the performance of an adsorption-based hydrogen storage system', *AlChE J.,* **55**, 2985-2996 (2009).

(22) Y. Li and R. T. Yang, 'Hydrogen storage on platinum nanoparticles doped on superactivated carbon', *J. Phys. Chem. C,* **111**, 11086-11094 (2007).

(23) N. P. Stadie, J. J. Purewal, C. C. Ahn, and B. Fultz, 'Measurements of hydrogen spillover in platinum doped superactivated carbon', *Langmuir,* **26**, 15481-15485 (2010).

(24) J. J. Purewal, H. Kabbour, J. J. Vajo, C. C. Ahn, and B. Fultz, 'Pore size distribution and supercritical hydrogen adsorption in activated carbon fibers', *Nanotechnology,* **20**, 204012 (2009).

(25) J. B. Dumas, 'A method of estimating nitrogen in organic material', *Ann. Chim. et Phys.,* **58**, 171 (1833).

(26) Z. Yang, Y. Xia, and R. Mokaya, 'Enhanced hydrogen storage capacity of high surface area zeolite-like carbon materials', *J. Am. Chem. Soc.,* **129**, 1673-1679 (2007).

(27) F. O. Mertens, 'Determination of absolute adsorption in highly ordered porous media', *Surf. Sci.,* **603**, 1979-1984 (2009).

(28) J. M. Obrecht, R. J. Wild, M. Antezza, L. P. Pitaevskii, S. Stringari, and E. A. Cornell, 'Measurement of the temperature dependence of the Casimir-Polder force', *Phys. Rev. Lett.,* **98**, 063201 (2007).

(29) J. Purewal, D. Liu, A. Sudik, M. Veenstra, J. Yang, S. Maurer, U. Müller, and D. J. Siegel, 'Improved hydrogen storage and thermal conductivity in high-density MOF-5 composites', *J. Phys. Chem. C,* **116**, 20199-20212 (2012).